Analysis of Two Spherical Parallel Manipulators With Hidden Revolute Joints

Ju Li
School of Mechanical Engineering,
Changzhou University,
Changzhou, Jiangsu 213164, China
e-mail: wangju0209@163.com

J. Michael McCarthy[1]
Department of Mechanical and
Aerospace Engineering,
University of California, Irvine,
Irvine, CA 92697
e-mail: jmmccart@uci.edu

In this paper, we examine two spherical parallel manipulators (SPMs) constructed with legs that include planar and spherical subchains that combine to impose constraints equivalent to hidden revolute joints. The first has supporting serial chain legs constructed from three revolute joints with parallel axes, denoted R‖R‖R, followed by two revolute joints that have intersecting axes, denoted $\widehat{RR}$. The leg has five degrees-of-freedom and is denoted R‖R‖R-$\widehat{RR}$. Three of these legs can be assembled so the spherical chains all share the same point of intersection to obtain a spherical parallel manipulator denoted as 3-R‖R‖R-$\widehat{RR}$. The second spherical parallel manipulator has legs constructed from three revolute joints that share one point of intersection, denoted $\widehat{RRR}$, and a second pair of revolute joints with axes that intersect in a different point. This five-degree-of-freedom leg is denoted $\widehat{RRR}$-$\widehat{RR}$. The spherical parallel manipulator constructed from these legs is 3-$\widehat{RRR}$-$\widehat{RR}$. We show that the internal constraints of these two types of legs combine to create hidden revolute joints that can be used to analyze the kinematics and singularities of these spherical parallel manipulators. A quaternion formulation provides equations for the quartic singularity varieties some of which decompose into pairs of quadric surfaces which we use to classify these spherical parallel manipulators.
[DOI: 10.1115/1.4035542]

Keywords: spherical parallel manipulator, forward kinematics, singularity variety, Jacobian matrix, dual quaternions, homogeneous polynomial

1 Introduction

Spherical parallel manipulators (SPMs) provide control of three degrees-of-freedom in orientation which is useful in a wide range of applications such as orienting devices [1], robotic wrists [2–5], robotic surgery [6], and human joint rehabilitation [7]. Recent research in the type synthesis of spherical parallel manipulators has yielded a large number of specialized devices that rely on geometric constraints in the supporting legs. In this paper, we study two structures that have internal constraints that combine to form hidden revolute joints. Once these joints are identified, the analysis of these spherical parallel manipulators is simplified.

The two structures that we examine in this paper arise in the work of Yang [8], who uses "position and orientation characteristic (POC)" of the motion output link (e.g., moving platform of a parallel mechanism, end link of a serial mechanism, etc.) to identify new structures for spherical parallel manipulators, two of which shown in Figs. 1 and 2. About the same time, Kong and Gosselin [9] uses screw theory for type synthesis and obtained the equivalent spherical parallel mechanisms, Fig. 3.

In the first case, each leg has a series of three revolute joints that form a planar chain, denoted R‖R‖R, and two more revolute joints that have axes that intersect, denoted $\widehat{RR}$, Fig. 1. When three of these legs are assembled so the ending $\widehat{RR}$ chains share the same point of intersection, O', the result is a three-degree-of-freedom 3-R‖R‖R-$\widehat{RR}$ spherical parallel manipulator.

In the second case, each leg is constructed from a series of three revolute joints that form a spherical chain with center O'_i, $i = 1,2,3$, denoted $\widehat{RRR}$, and two more revolute joints that have axes that intersect, $\widehat{RR}$, Fig. 2. When three of these legs are assembled so the ending $\widehat{RR}$ chains share the same point of intersection, O', the result is a three-degree-of-freedom 3-$\widehat{RRR}$-$\widehat{RR}$ spherical parallel manipulator [8].

Kong and Gosselin [9] have the same structures as those presented by Yang [8], but use the notation $(RRR)^E$ and $(RRR)^S$ to denote a planar and spherical RRR chains, respectively, and $\check{R}\check{R}$ to denote the intersection of the two ending revolute joints. They denote these spherical parallel manipulators as 3-$(RRR)^E$-$\check{R}\check{R}$ and 3-$(RRR)^S$-$\check{R}\check{R}$, respectively, Fig. 3.

Our goal is to analyze the forward kinematics and singularity varieties of the 3-R‖R‖R-$\widehat{RR}$ and 3-$\widehat{RRR}$-$\widehat{RR}$ spherical parallel

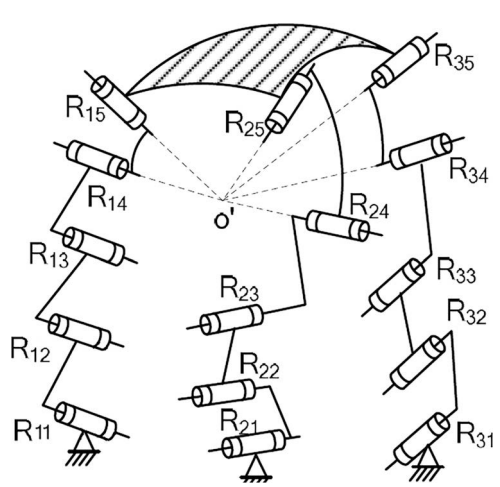

Fig. 1 The spherical parallel manipulator, 3-R‖R‖R-$\widehat{RR}$, consisting of three revolute joints that form a planar chain followed by two revolute joints with axes that intersect. The three legs are assembled so the axes of the end pairs of revolute joints intersect at O′.

[1]Corresponding author.

Manuscript received July 26, 2016; final manuscript received December 13, 2016; published online March 22, 2017. Assoc. Editor: Shaoping Bai.

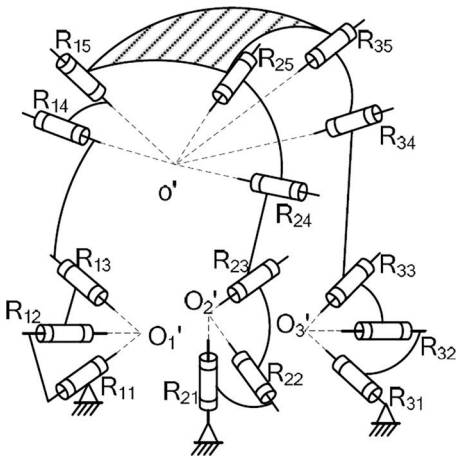

Fig. 2 The spherical parallel manipulator, 3-$\widehat{\text{RRR}}$-$\widehat{\text{RR}}$, formed from three revolute joints with axes that intersect in one point and two more revolute joints with axes that intersect. The three legs are assembled so the axes of the end pairs of revolute joints intersect at O′.

manipulators, which include internal constraints on each leg formed from planar and spherical subchains. We show that these planar and spherical subchains create hidden revolute joints that, once identified, simplify the analysis. The result is the constraint manifolds for these spherical parallel manipulators as the intersection of quadrics in quaternion coordinates. The Dixon resultant is used to solve the forward kinematic equations. And we obtain the singularity varieties of the general versions of these spherical parallel manipulators and their special cases.

2 Literature Review

The study of spherical parallel manipulators has shown that the forward kinematic equations of a general SPM have eight solutions [10,11]. Huang and Yao [12] used actuation joint angles as unknowns in solving the forward kinematics and a closed-form solution for a specific structure was obtained. Bai et al. [13] proposed a robust forward kinematic analysis by representing the SPMs using two spherical four-bar linkages. Kong and Gosselin [14] proposed a simple kinematics equation to calculate the unique solution of the Agile eye. Zhang et al. [15] analyzed the kinematics performance of a new orthogonal spherical parallel mechanism. Gan et al. [16] studied the forward kinematics solution distribution and analytic singularity-free workspace of linear-actuated symmetrical spherical parallel manipulators.

Gosselin and Angeles [17] were the first to study the singularities of general parallel manipulators and introduced two Jacobian matrices that define input and output velocities. Bonev and Gosselin [18] presented the computation and representation of the type 2 singularity loci of symmetric spherical parallel mechanisms based on an intuitive orientation representation. Sefrioui and Gosselin [19] studied the singularity loci of general three-degree-of-freedom planar parallel manipulators and obtained a graphical representation of these loci in the manipulator's workspace. Collin and McCarthy [20] studied the workspace and singular configurations of a planar platform supported by three linearly actuated legs, the 3-RPR parallel manipulator. Collin and McCarthy [21] then studied the Jacobian of spatial parallel manipulators that have triangular base and top platform architectures with 2-2-2 and 3-2-1 actuator configurations. Yu et al. [22] made a comparative study on motion characteristics of three two-degree-of-freedom pointing mechanisms.

This paper analyzes the 3-R‖R‖R-$\widehat{\text{RR}}$ and 3-$\widehat{\text{RRR}}$-$\widehat{\text{RR}}$ spherical parallel manipulators that have legs with planar and spherical subchains that combine to impose hidden revolute joints. Using these hidden joints, we obtain the forward kinematics and Jacobian of these manipulators. A precursor to this work is Kong and Gosselin [23], who generate alternative spherical parallel mechanisms by removing joints. What we show here is that to analyze these systems, we must identify and recreate these hidden revolute joints.

3 The Hidden Revolute Joint

In this section, we show how internal geometric constraints on each leg of a 3-R‖R‖R-$\widehat{\text{RR}}$ spherical parallel manipulator introduce the equivalent of a hidden revolute joint. Intersection of the motion subgroups [24] for the planar and spherical subchains of these legs suggests the existence of a shared axis, and in what follows we provide a detailed calculation to identify this hidden revolute joint and its properties. A similar analysis can be applied to

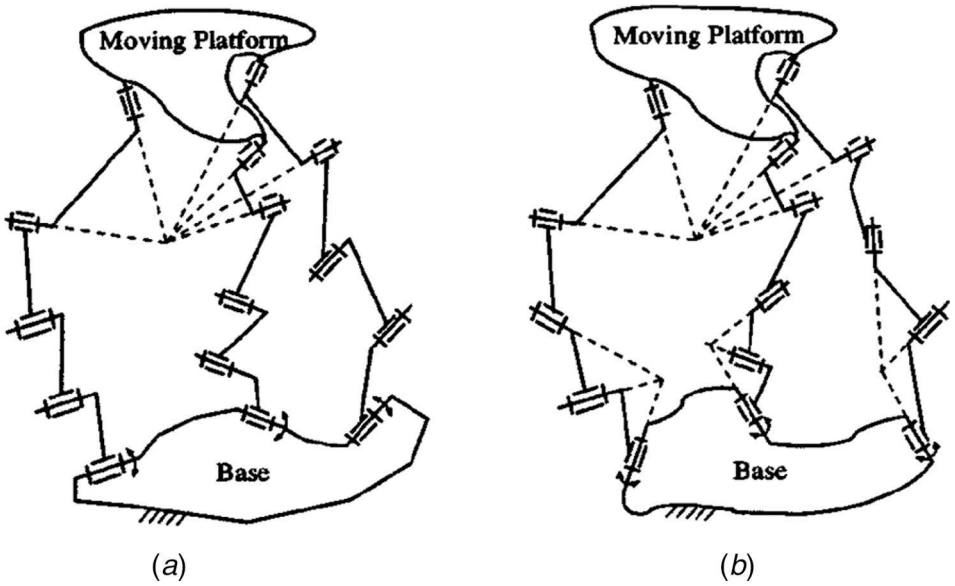

Fig. 3 Spherical parallel manipulators by Kong and Gosselin [9] that have the same structure as the 3-R‖R‖R-$\widehat{\text{RR}}$ and 3-$\widehat{\text{RRR}}$-$\widehat{\text{RR}}$, denoted (*a*) 3-$(\text{RRR})^{E}$-$\check{\text{R}}\check{\text{R}}$ and (*b*) 3-$(\text{RRR})^{S}$-$\check{\text{R}}\check{\text{R}}$

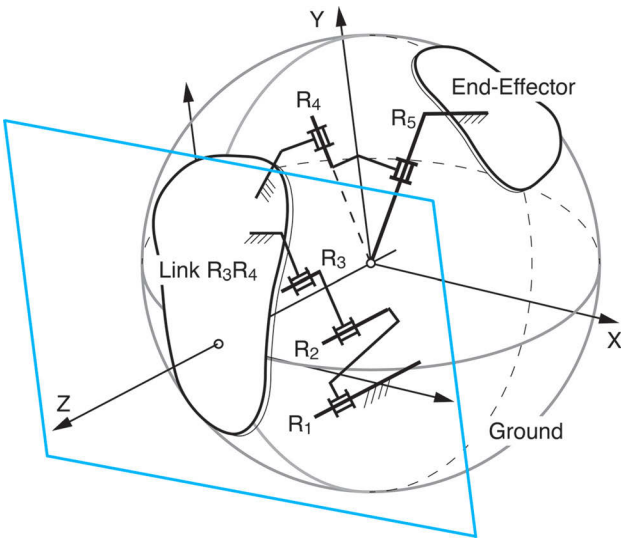

Fig. 4 The link R_3R_4 connects the planar and spherically constrained portions of the 3-R‖R‖R-$\widehat{\text{RR}}$

the legs of the 3-$\widehat{\text{RRR}}$-$\widehat{\text{RR}}$ spherical parallel manipulator in order to identify its hidden revolute joint.

Consider the 5R serial chain shown in Fig. 4, which forms one leg of this spherical parallel manipulator. This leg has the internal geometric constraints: (i) the subchain chain $R_1R_2R_3$ forms a planar chain such that each link moves in planes perpendicular to the Z axis of the ground frame F; and (ii) the remaining joints of the subchain chain R_4R_5 are required to intersect at the origin of F such that the links of this chain are constrained to move on concentric spheres around this point.

Of particular interest is the movement of the link denoted R_3R_4, which must satisfy both constraints, that moves on a plane perpendicular to the Z axis and on a sphere around the origin of the ground frame F. We use dual quaternions to define the movement of this link [25,26].

A dual quaternion, $\widehat{A}$ is formed from a pair of quaternions, A and U, written as, $\widehat{A} = A + \varepsilon U$. A quaternion has four real components, $A = (a_1, a_2, a_3, a_4)$, and the product of two quaternions AB has the four components given by the matrix operation

$$AB = \begin{bmatrix} a_4 & -a_3 & a_2 & a_1 \\ a_3 & a_4 & -a_1 & a_2 \\ -a_2 & a_1 & a_3 & a_4 \\ -a_1 & -a_2 & -a_3 & a_4 \end{bmatrix} \begin{Bmatrix} b_1 \\ b_2 \\ b_3 \\ b_4 \end{Bmatrix} \tag{1}$$

This definition of the quaternion product simplifies its calculation and avoids Hamilton's quaternion units, i, j, and k [26].

The product of two dual quaternions $\widehat{A} = A + \varepsilon U$ and $\widehat{B} = B + \varepsilon V$ is given by

$$\widehat{A}\widehat{B} = (A + \varepsilon U)(B + \varepsilon V) = AB + \varepsilon(AV + UB) \tag{2}$$

This operation can be viewed as multiplication with the condition $\varepsilon^2 = 0$, see Ref. [25].

The movement of the link R_3R_4, as constrained by the planar chain $R_1R_2R_3$, is defined by the dual quaternion $\widehat{P}$ that is the product of translations by a and b in the X and Y directions, respectively, and a rotation θ about the Z direction

$$\begin{aligned} \widehat{X}_{\text{trans}}(a) &= (0, 0, 0, 1) + \varepsilon(a/2, 0, 0, 0) \\ \widehat{Y}_{\text{trans}}(b) &= (0, 0, 0, 1) + \varepsilon(0, b/2, 0, 0) \\ \widehat{Z}_{\text{rot}}(\theta) &= (0, 0, \sin\theta/2, \cos\theta/2) \end{aligned} \tag{3}$$

which yields

$$\begin{aligned} \widehat{P} &= \widehat{X}_{\text{trans}}(a)\widehat{Y}_{\text{trans}}(b)\widehat{Z}_{\text{rot}}(\theta) \\ &= (0, 0, \sin\theta/2, \cos\theta/2) \\ &\quad + \varepsilon\left(\frac{a}{2}\cos\theta/2 + \frac{b}{2}\sin\theta/2, -\frac{a}{2}\sin\theta/2 + \frac{b}{2}\cos\theta/2, 0, 0\right) \end{aligned} \tag{4}$$

Now the movement of link R_3R_4 as constrained by the spherical chain R_4R_5 is defined by the dual quaternion $\widehat{S}$ that is the product of a rotation λ about the Y axis, a rotation of $-\mu$ around the X axis and a rotation ϕ about the Z axis

$$\begin{aligned} \widehat{Y}_{\text{rot}}(\lambda) &= (0, \sin\lambda/2, 0, \cos\lambda/2) \\ \widehat{X}_{\text{rot}}(-\mu) &= (-\sin\mu/2, 0, 0, \cos\mu/2) \\ \widehat{Z}_{\text{rot}}(\phi) &= (0, 0, \sin\phi/2, \cos\phi/2) \end{aligned} \tag{5}$$

which yields

$$\begin{aligned} \widehat{S} &= \widehat{Y}_{\text{rot}}(\lambda)\widehat{X}_{\text{rot}}(-\mu)\widehat{Z}_{\text{rot}}(\phi) \\ &= \Bigg(-\cos\frac{\lambda}{2}\cos\frac{\phi}{2}\sin\frac{\mu}{2} + \cos\frac{\mu}{2}\sin\frac{\lambda}{2}\sin\frac{\phi}{2} \\ &\quad \times \cos\frac{\mu}{2}\cos\frac{\phi}{2}\sin\frac{\lambda}{2} + \cos\frac{\lambda}{2}\sin\frac{\mu}{2}\sin\frac{\phi}{2} \\ &\quad \times \cos\frac{\phi}{2}\sin\frac{\lambda}{2}\sin\frac{\mu}{2} + \cos\frac{\lambda}{2}\cos\frac{\mu}{2}\sin\frac{\phi}{2} \\ &\quad \times \cos\frac{\lambda}{2}\cos\frac{\mu}{2}\cos\frac{\phi}{2} - \sin\frac{\lambda}{2}\sin\frac{\mu}{2}\sin\frac{\phi}{2}\Bigg) \end{aligned} \tag{6}$$

The angles λ and μ can be interpreted as longitude and latitude angles of the position of the local z axis of rotation for this spherical movement.

In order for the link R_3R_4 to be able to move in a way that satisfies both the planar chain $R_1R_2R_3$ and the spherical chain R_4R_5, we must have

$$\widehat{P} = \widehat{S} \tag{7}$$

This shows that $a = b = 0$, $\lambda = \mu = 0$, and $\theta = \phi$. Thus, to satisfy the geometric constraints imposed on this leg, the movement of the link R_3R_4 is given

$$\widehat{P} = \widehat{S} = (0, 0, \sin\theta/2, \cos\theta/2) \tag{8}$$

which is a pure rotation about the ground Z axis. This rotation is equivalent to the presence of a revolute joint that attaches link R_3R_4 to the fixed frame. We call this a *hidden* revolute joint that arises from the geometric constraints of the R‖R‖R-$\widehat{\text{RR}}$ leg as part of the 3-R‖R‖R-$\widehat{\text{RR}}$ spherical parallel manipulator.

This hidden revolute joint can be identified for each of the R‖R‖R-$\widehat{\text{RR}}$ legs no matter how they are positioned. The axis of this joint passes through the center defined by the movement of the spherical chain and is in the direction perpendicular to the plane of movement of the planar chain. The existence of the hidden revolute joint shows that the movement of the leg is equivalent to an end-effector supported by spherical 3R chain $R_{iH}R_{i4}R_{i5}$, that has its base link $R_{i4}R_{iH}R_{i3}$ which is the output link of the planar four-bar linkage $R_{i1}R_{i2}R_{i3}R_{iH}$, $i = 1, 2, 3$, Fig. 5.

A similar analysis for the 3-$\widehat{\text{RRR}}$-$\widehat{\text{RR}}$ spherical parallel manipulator shows that the link $R_{i3}R_{i4}$ must rotate around the axis that passes through the center of the spherical chain $R_{i1}R_{i2}R_{i3}$ and the spherical chain $R_{i4}R_{i5}$. This hidden revolute joint combines with $R_{i4}R_{i5}$ to form a spherical 3R chain that supports the end-effector, and the base link $R_{i4}R_{iH}R_{i3}$ is driven by the spherical four-bar linkage $R_{i1}R_{i2}R_{i3}R_{iH}$, $i = 1, 2, 3$, Fig. 6.

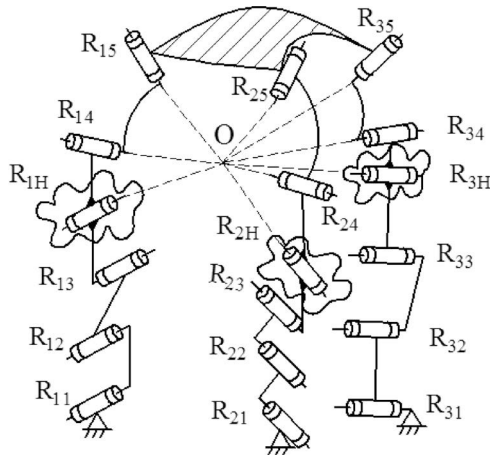

Fig. 5 The platform is supported by three spherical 3*R* chains $R_{iH}R_{i4}R_{i5}$, and each base link $R_{i4}R_{iH}R_{i3}$ is driven by the planar four-bar linkage $R_{i1}R_{i2}R_{i3}R_{iH}$. The revolute joints R_{iH}, $i=1,2,3$, denote the hidden revolute joints.

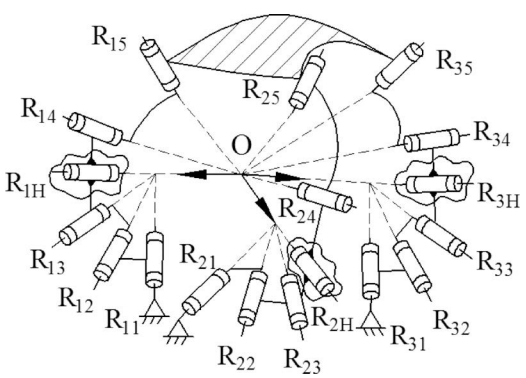

Fig. 6 The platform is supported by three spherical 3*R* chains $R_{iH}R_{i4}R_{i5}$, and each base link $R_{i4}R_{iH}R_{i3}$ is driven by the spherical 4*R* linkage $R_{i1}R_{i2}R_{i3}R_{iH}$. The revolute joints R_{iH}, $i=1,2,3$, denote the hidden revolute joints.

In both cases, the dimensions of the equivalent 3-$\widehat{\text{RRR}}$ spherical parallel manipulator that includes the hidden revolute joints is used to analyze the movement of the 3-R‖R‖R-$\widehat{\text{RR}}$ and 3-$\widehat{\text{RRR}}$-$\widehat{\text{RR}}$ spherical parallel manipulators.

4 Constraint Manifold of the 3-$\widehat{\text{RRR}}$ Manipulator

Since the hidden revolute joints can be identified for both the 3-R‖R‖R-$\widehat{\text{RR}}$ and the 3-$\widehat{\text{RRR}}$-$\widehat{\text{RR}}$ spherical parallel manipulators no matter how they are positioned, we just study the constraint manifold of the equivalent 3-$\widehat{\text{RRR}}$ spherical parallel manipulator that includes the hidden revolute joints.

The diagram of the equivalent 3-$\widehat{\text{RRR}}$ manipulator is shown in Fig. 7, where $\mathbf{u}_i$, $\mathbf{w}_i$, $\mathbf{v}_i$, $i=1,2,3$, denote the unit vectors along the axes of joints R_{iH}, R_{i4}, and R_{i5}, respectively, and μ_i is the angle between axes $\mathbf{u}_i$ and $\mathbf{w}_i$, while τ_i is the angle between axes $\mathbf{w}_i$ and $\mathbf{v}_i$. We assign a O-XYZ coordinates connected with the fixed platform, and a O-$x_0y_0z_0$ coordinates connected with the moving platform at the centered point O. Let the positions of the fixed pivots be specified by $\mathbf{u}_i=(x_i,y_i,z_i)$, $i=1,2,3$, measured in the fixed frame F and the moving pivots be $\mathbf{v}_{i0}=(r_i,s_i,t_i)$, $i=1,2,3$, measured in the moving frame M.

The position and orientation of the end-effector of the manipulator is defined by the coordinate transformation of points $\mathbf{z}_0$ in a moving frame M to coordinates $\mathbf{z}$ in a fixed frame F given by

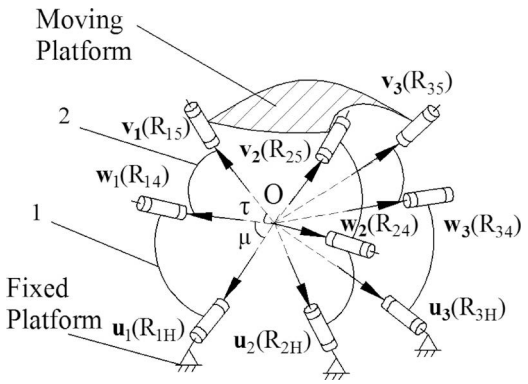

Fig. 7 The 3-$\widehat{\text{RRR}}$ manipulator. $\mathbf{u}_i$, $\mathbf{w}_i$, $\mathbf{v}_i$, $i=1,2,3$, denote the unit vectors along the axes of joints R_{iH}, R_{i4}, and R_{i5}, respectively, and μ_i is the angle between axes $\mathbf{u}_i$ and $\mathbf{w}_i$, while τ_i is the angle between axes $\mathbf{w}_i$ and $\mathbf{v}_i$.

$$\mathbf{z}=[\boldsymbol{R}]\mathbf{z}_0+\mathbf{d} \tag{9}$$

The matrix $[\boldsymbol{R}]$ is a 3×3 rotation matrix and the vector $\mathbf{d}=(d_x,d_y,d_z)$ is the 3×1 translation vector that defines the position of reference frame M relative to F.

The rotation matrix $[\boldsymbol{R}]$ and translation vector $\mathbf{d}$ in Eq. (9) can be defined in terms of dual quaternion coordinates [26] given by

$$[\boldsymbol{R}]=\begin{bmatrix} q_1^2-q_2^2-q_3^2+q_4^2 & 2(q_1q_2-q_3q_4) & 2(q_1q_3+q_2q_4) \\ 2(q_1q_2+q_3q_4) & -q_1^2+q_2^2-q_3^2+q_4^2 & 2(q_2q_3-q_1q_4) \\ 2(q_1q_3-q_2q_4) & 2(q_2q_3+q_1q_4) & -q_1^2-q_2^2+q_3^2+q_4^2 \end{bmatrix} \tag{10}$$

and

$$\mathbf{d}=2\begin{bmatrix} -q_8 & q_7 & -q_6 & q_5 \\ -q_7 & -q_8 & q_5 & q_6 \\ q_6 & -q_5 & -q_8 & q_7 \end{bmatrix}\begin{Bmatrix} q_1 \\ q_2 \\ q_3 \\ q_4 \end{Bmatrix} \tag{11}$$

Since the moving platform of the spherical 3-$\widehat{\text{RRR}}$ parallel manipulator can only rotate around the point O of the fixed platform, we choose the point O as the origin of the fixed and moving frames, then, the translation vector $\mathbf{d}$ is zero. Then, the vector $\mathbf{v}_{i0}$ defined in the moving frame can be transformed to the corresponding vector $\mathbf{v}_i$ defined in the fixed frame by

$$\mathcal{C}_i: \quad \mathbf{v}_i=[\boldsymbol{R}]\mathbf{v}_{i0}, \quad i=1,2,3 \tag{12}$$

Let the angle between axes $\mathbf{u}_i$ and $\mathbf{v}_i$ be ρ_i, then, we have three constraint equations for the spherical platform

$$\mathcal{C}_i: \quad \mathbf{u}_i^{\mathrm{T}}\mathbf{v}_i=\mathbf{u}_i^{\mathrm{T}}[\boldsymbol{R}]\mathbf{v}_{i0}=\cos\rho_i, \quad i=1,2,3 \tag{13}$$

These equations can be interpreted as constraints on vectors with quaternion components $\mathbf{q}=(q_1,q_2,q_3,q_4)$. It is convenient to write Eq. (13) as the quadratic forms

$$\mathcal{C}_i: \quad \mathbf{q}^{\mathrm{T}}[C_i]\mathbf{q}=\cos\rho_i, \quad i=1,2,3 \tag{14}$$

where $[\boldsymbol{C}_i]$ is a symmetric 4×4 matrix with the upper triangular coefficients given by

$$
\begin{aligned}
C_{11i} &= x_i r_i - y_i s_i - z_i t_i \\
C_{12i} &= r_i y_i + x_i s_i \\
C_{13i} &= r_i z_i + x_i t_i \\
C_{14i} &= s_i z_i - y_i t_i \\
C_{22i} &= -x_i r_i + y_i s_i - z_i t_i \\
C_{23i} &= r_i z_i + y_i t_i \\
C_{24i} &= -r_i z_i + x_i t_i \\
C_{33i} &= -x_i r_i - y_i s_i + z_i t_i \\
C_{34i} &= r_i y_i - x_i s_i \\
C_{44i} &= x_i r_i + y_i s_i + z_i t_i, \quad i = 1,2,3
\end{aligned} \tag{15}
$$

The intersection of the three quadric equations in quaternion coordinates defines the constraint manifold of the spherical platform.

5 Forward Kinematics Analysis

For either of the planar 4*R* driving linkage of the 3-R‖R‖R-$\widehat{\text{RR}}$ manipulator in Fig. 5 or the spherical 4*R* driving linkage of the 3-$\widehat{\text{RRR}}$-$\widehat{\text{RR}}$ mechanism shown in Fig. 6, we can identify a driving link $R_{i1}R_{i2}$ and an output link $R_{i3}R_{iH}$. Given the input angle θ of the driving link, we can obtain the output angle ψ of the output link [25]

$$
\psi(\theta) = \arctan\left(\frac{B}{A}\right) \pm \arccos\left(\frac{C}{\sqrt{A^2+B^2}}\right) \tag{16}
$$

where, for the planar 4*R* driving linkage

$$
\begin{aligned}
&A(\theta) = 2ab\cos\theta - 2gb, \quad B(\theta) = 2ab\sin\theta, \\
&C(\theta) = g^2 + b^2 + a^2 - h^2 - 2ag\cos\theta
\end{aligned} \tag{17}
$$

where a, h, b, and g denote the link lengths of the links $R_{i1}R_{i2}$, $R_{i2}R_{i3}$, $R_{i3}R_{iH}$, and $R_{i1}R_{iH}$, respectively, which define the dimensions of the 4*R* planar linkage. For the spherical 4*R* driving linkage

$$
\begin{aligned}
A(\theta) &= \cos\theta\sin\alpha\cos\gamma\sin\beta - \cos\alpha\sin\gamma\sin\beta \\
B(\theta) &= \sin\theta\sin\alpha\sin\beta \\
C(\theta) &= \cos\eta - \cos\theta\sin\alpha\sin\gamma\cos\beta - \cos\alpha\cos\gamma\cos\beta
\end{aligned} \tag{18}
$$

where α, β, γ, and η denote the angular lengths of the links $R_{i1}R_{i2}$, $R_{i2}R_{i3}$, $R_{i3}R_{iH}$, and $R_{i1}R_{iH}$, respectively, which define the dimensions of the 4*R* spherical linkage.

For the convenience of analysis, let the axes of the three hidden revolute joints R_{1H}, R_{2H}, and R_{3H} in Fig. 7 be perpendicular to each another, and let the axes of three revolute joints R_{15}, R_{25}, and R_{35} which connect with the moving platform be perpendicular to each another. We assign the *X*, *Y*, *Z* axes of fixed frame *O*-*XYZ* in coincidence with the $\mathbf{u}_1$, $\mathbf{u}_2$, $\mathbf{u}_3$ axes, and the x_0, y_0, z_0 axes of moving frame O-$x_0y_0z_0$ in coincidence with the $\mathbf{v}_2$, $\mathbf{v}_3$, $\mathbf{v}_1$ axes, respectively. As the link 1 of each leg rotates an angle ψ_i, the vector of the corresponding branched intermediate axis $\mathbf{w}_i$ relative to the fixed frame *F* is given by [25]

$$
\begin{aligned}
\mathbf{w}_1 &= (\cos\mu_1,\ \cos\psi_1\sin\mu_1,\ \sin\psi_1\sin\mu_1), \\
\mathbf{w}_2 &= (\sin\psi_2\sin\mu_2,\ \cos\mu_2,\ \cos\psi_2\sin\mu_2), \\
\mathbf{w}_3 &= (\cos\psi_3\sin\mu_3,\ \sin\psi_3\sin\mu_3,\ \cos\mu_3)
\end{aligned} \tag{19}
$$

Let the moving unit vectors $\mathbf{v}_i$ be specified by

$$
\mathbf{v}_{10} = (0,0,1), \quad \mathbf{v}_{20} = (1,0,0), \quad \mathbf{v}_{30} = (0,1,0) \tag{20}
$$

measured in the moving frame *M*. Then, the three constraint equations for the spherical platform can be written as

$$
\mathcal{C}_i: \quad \mathbf{w}_i^{\mathrm{T}}\mathbf{v}_i = \mathbf{w}_i^{\mathrm{T}}[\boldsymbol{R}]\mathbf{v}_{i0} = \cos\tau_i, \quad i = 1,2,3 \tag{21}
$$

It is convenient to write Eq. (21) as the quadratic forms

$$
\mathcal{C}_i: \quad \mathbf{q}^{\mathrm{T}}[\boldsymbol{D}_i]\mathbf{q} = 0, \quad i = 1,2,3 \tag{22}
$$

The symmetric 4×4 matrices, $[\boldsymbol{D}_i], i = 1,2,3$, are given by

$$
[\boldsymbol{D}_1] = \begin{bmatrix}
-c\tau_1 - s\mu_1 s\psi_1 & 0 & c\mu_1 & -c\psi_1 s\mu_1 \\
0 & -c\tau_1 - s\mu_1 s\psi_1 & c\psi_1 s\mu_1 & c\mu_1 \\
c\mu_1 & c\psi_1 s\mu_1 & -c\tau_1 + s\mu_1 s\psi_1 & 0 \\
-c\psi_1 s\mu_1 & c\mu_1 & 0 & -c\tau_1 + s\mu_1 s\psi_1
\end{bmatrix} \tag{23}
$$

$$
[\boldsymbol{D}_2] = \begin{bmatrix}
-c\tau_2 + s\mu_2 s\psi_2 & c\mu_2 & c\psi_2 s\mu_2 & 0 \\
c\mu_2 & -c\tau_2 - s\mu_2 s\psi_2 & 0 & -c\psi_2 s\mu_2 \\
c\psi_2 s\mu_2 & 0 & -c\tau_2 - s\mu_2 s\psi_2 & c\mu_2 \\
0 & -c\psi_2 s\mu_2 & c\mu_2 & -c\tau_2 + s\mu_2 s\psi_2
\end{bmatrix} \tag{24}
$$

and

$$
[\boldsymbol{D}_3] = \begin{bmatrix}
-c\tau_3 - s\mu_3 s\psi_3 & c\psi_3 s\mu_3 & 0 & c\mu_3 \\
c\psi_3 s\mu_3 & -c\tau_3 + s\mu_3 s\psi_3 & c\mu_3 & 0 \\
0 & c\mu_3 & -c\tau_3 - s\mu_3 s\psi_3 & -c\psi_3 s\mu_3 \\
c\mu_3 & 0 & -c\psi_3 s\mu_3 & -c\tau_3 + s\mu_3 s\psi_3
\end{bmatrix} \tag{25}
$$

Table 1 Solutions of 3-R||R||R-$\widehat{\text{RR}}$ spherical parallel manipulator with $a=1$ mm, $b=h=2$ mm, $g=3$ mm, $\mu_1=\mu_2=\mu_3=90$ deg, $\tau_1=\tau_2=\tau_3=45$ deg, $\theta_1=\theta_2=\theta_3=60$ deg

	p_1	p_2	p_3
1	-0.133655	-0.133655	-0.133655
2	-1.86405	-1.86405	-1.86405
3	$0.123025-0.181317\,i$	$-0.836312-0.552749\,i$	$-0.711599-0.0465637\,i$
4	$0.123025+0.181317\,i$	$-0.836312+0.552749\,i$	$-0.711599+0.0465637\,i$
5	$-0.836312+0.552749\,i$	$-0.711599+0.0465637\,i$	$0.123025+0.181317\,i$
6	$-0.836312-0.552749\,i$	$-0.711599-0.0465637\,i$	$0.123025-0.181317\,i$
7	$-0.711599-0.0465637\,i$	$0.123025-0.181317\,i$	$-0.836312-0.552749\,i$
8	$-0.711599+0.0465637\,i$	$0.123025+0.181317\,i$	$-0.836312+0.552749\,i$

where s and c denote the sine and cosine functions.

We dehomogenize the quaternion coordinates in Eq. (22) with respect to q_4. This is done by making the substitution

$$p_1 = q_1/q_4, \quad p_2 = q_2/q_4, \quad p_3 = q_3/q_4 \tag{26}$$

Then, Eq. (22) can be seen as the functions of p_1, p_2 by putting the products of power in p_3 into the coefficients

$$\mathcal{C}_i: \quad f_i(1, p_1, p_2, p_1p_2, p_1^2, p_2^2) = 0, \quad i = 1,2,3 \tag{27}$$

According to Dixon's resultant principle, we introduce two new variables t_1 and t_2 and form the Dixon determinant

$$\Delta(p_1,p_2,t_1,t_2) = \begin{vmatrix} f_1(p_1,p_2) & f_2(p_1,p_2) & f_3(p_1,p_2) \\ f_1(t_1,p_2) & f_2(t_1,p_2) & f_3(t_1,p_2) \\ f_1(t_1,t_2) & f_2(t_1,t_2) & f_3(t_1,t_2) \end{vmatrix} \tag{28}$$

Dixon observed that Δ vanishes when $t_1=p_1$ and $t_2=p_2$, which implies that $(p_1-t_1)(p_2-t_2)$ are factors of Δ. Divide out these factors to obtain the Dixon polynomial δ

$$\delta(p_1,p_2,t_1,t_2) = \frac{\Delta(p_1,p_2,t_1,t_2)}{(p_1-t_1)(p_2-t_2)} = 0 \tag{29}$$

The polynomial Eq. (29) can be rewritten as

$$\delta(p_1,p_2,t_1,t_2) = \frac{\Delta(p_1,p_2,t_1,t_2)}{(p_1-t_1)(p_2-t_2)} = \mathbf{T}^{\mathrm{T}}[\boldsymbol{D}]\mathbf{C} = 0 \tag{30}$$

where $\mathbf{T}^{\mathrm{T}} = (t_1^2, t_1t_2, t_1, t_2, 1)$, $\mathbf{C}^{\mathrm{T}} = (p_2^2, p_1p_2, p_1, p_2, 1)$, $[\boldsymbol{D}]$ is a matrix whose elements are polynomials in p_3.

Dixon proved that three functions in Eq. (27) have common zeros if the determinant of the matrix $[\boldsymbol{D}]$ equals to 0.

$$\det[\boldsymbol{D}] = 0 \tag{31}$$

Then, a univariate equation in p_3 of degree 8 is obtained

$$\sum_{j=0}^{+8} c_j p_3^j = 0 \tag{32}$$

where the coefficients c_j are functions of the geometric parameters of the manipulator and of the actuator angles. Then, eight sets of solutions for the forward kinematic equations can be obtained.

To illustrate the above result, an example of the manipulator is presented. The geometric parameters and the actuator angles of the 3-R||R||R-$\widehat{\text{RR}}$ spherical parallel manipulator are given as $a=1$ mm, $b=h=2$ mm, $g=3$ mm, $\mu_1=\mu_2=\mu_3=90$ deg, $\tau_1=\tau_2=\tau_3=45$ deg, $\theta_1=\theta_2=\theta_3=60$ deg, while eight sets of solutions obtained are listed in Table 1.

6 Singularities

In order to determine the singularities of the spherical platform, we collect the quadratic Eq. (14) that define the constraint manifold together with the unit magnitude requirement for a vector $\mathbf{q}$ with quaternion components, to obtain

$$\mathbf{q}^{\mathrm{T}}[\boldsymbol{C}_1]\mathbf{q} = \cos\rho_1, \quad \mathbf{q}^{\mathrm{T}}[\boldsymbol{C}_2]\mathbf{q} = \cos\rho_2, \quad \mathbf{q}^{\mathrm{T}}[\boldsymbol{C}_3]\mathbf{q} = \cos\rho_3, \quad \mathbf{q}^{\mathrm{T}}\mathbf{q} = 1 \tag{33}$$

The time derivative of these four equations can be assembled into the matrix equation

$$\begin{bmatrix} \mathbf{q}^{\mathrm{T}}[\boldsymbol{C}_1] \\ \mathbf{q}^{\mathrm{T}}[\boldsymbol{C}_2] \\ \mathbf{q}^{\mathrm{T}}[\boldsymbol{C}_3] \\ q_1, q_2, q_3, q_4 \end{bmatrix} \begin{Bmatrix} \dot{q}_1 \\ \dot{q}_2 \\ \dot{q}_3 \\ \dot{q}_4 \end{Bmatrix} - \begin{bmatrix} -1/2\sin\rho_1 & 0 & 0 & 0 \\ 0 & -1/2\sin\rho_2 & 0 & 0 \\ 0 & 0 & -1/2\sin\rho_3 & 0 \\ 0 & 0 & 0 & 0 \end{bmatrix} \times \begin{Bmatrix} \dot{\rho}_1 \\ \dot{\rho}_2 \\ \dot{\rho}_3 \\ 0 \end{Bmatrix} = \begin{Bmatrix} 0 \\ 0 \\ 0 \\ 0 \end{Bmatrix} \tag{34}$$

which has the form of the Jacobian for a parallel manipulator

$$[\boldsymbol{A}]\dot{\mathbf{q}} - [\boldsymbol{B}]\dot{\mathbf{r}} = 0 \tag{35}$$

where $\dot{\mathbf{q}} = (\dot{q}_1, \dot{q}_2, \dot{q}_3, \dot{q}_4)$ and $\dot{\mathbf{r}} = (\dot{\rho}_1, \dot{\rho}_2, \dot{\rho}_3, 0)$. The configurations of the manipulator for which the determinant of the coefficient matrix $[\boldsymbol{A}]$ is zero are known as "type 2 singularities" of the manipulator [17].

The elements of $[\boldsymbol{A}]$ in Eq. (35) are linear in the quaternion coordinates $\mathbf{q} = (q_1, q_2, q_3, q_4)$ therefore

$$\mathcal{S}: \quad \det[\boldsymbol{A}] = 0 \tag{36}$$

defines a quartic algebraic manifold that we call the *singularity variety* of the manipulator.

6.1 Singularity Variety of the General 3-$\widehat{\text{RRR}}$.

Let the positions of pivots in the fixed and moving frames in Fig. 7 be specified as shown in Table 2. ϕ is the angle between axes $\mathbf{u}_1$ and $\mathbf{u}_2$, while δ is the angle between axes $\mathbf{v}_1$ and $\mathbf{v}_2$. λ is the angle between $\mathbf{u}_3$ axis and YOZ plane, while σ is the angle between $\mathbf{v}_3$ axis and y_0Oz_0 plane. ν is the angle between axis $\mathbf{u}_1$ and projection of axis $\mathbf{u}_3$ in YOZ plane, while ε is the angle between axis $\mathbf{v}_1$ and projection of axis $\mathbf{v}_3$ in y_0Oz_0 plane.

Substitute these positions into the matrix $[\boldsymbol{A}]$ of the Jacobian, to obtain

$$[\boldsymbol{A}] = \begin{bmatrix} -q_1 & -q_2 & q_3 & q_4 \\ G_1 & G_2 & G_3 & G_4 \\ G_5 & G_6 & G_7 & G_8 \\ q_1 & q_2 & q_3 & q_4 \end{bmatrix} \tag{37}$$

where

$$\begin{aligned}
G_1 &= q_4 \sin(\phi - \delta) - q_1 \cos(\phi - \delta) \\
G_2 &= -q_3 \sin(\phi + \delta) - q_2 \cos(\phi + \delta) \\
G_3 &= -q_2 \sin(\phi + \delta) + q_3 \cos(\phi + \delta) \\
G_4 &= q_1 \sin(\phi - \delta) + q_4 \cos(\phi - \delta) \\
G_5 &= q_4 \cos\lambda \cos\sigma \sin(\nu - \varepsilon) + q_3(\cos\varepsilon \cos\sigma \sin\lambda + \cos\lambda \cos\nu \sin\sigma) \\
&\quad - q_1[\cos\lambda \cos\sigma \cos(\nu - \varepsilon) - \sin\lambda \sin\sigma] - q_2(\cos\sigma \sin\lambda \sin\varepsilon + \cos\lambda \sin\nu \sin\sigma) \\
G_6 &= -q_3 \cos\lambda \cos\sigma \sin(\nu + \varepsilon) + q_4(\cos\varepsilon \cos\sigma \sin\lambda - \cos\lambda \cos\nu \sin\sigma) \\
&\quad - q_2[\cos\lambda \cos\sigma \cos(\nu + \varepsilon) + \sin\lambda \sin\sigma] - q_1(\cos\sigma \sin\lambda \sin\varepsilon + \cos\lambda \sin\nu \sin\sigma) \\
G_7 &= -q_2 \cos\lambda \cos\sigma \sin(\nu + \varepsilon) + q_1(\cos\varepsilon \cos\sigma \sin\lambda + \cos\lambda \cos\nu \sin\sigma) \\
&\quad + q_3[\cos\lambda \cos\sigma \cos(\nu + \varepsilon) - \sin\lambda \sin\sigma] + q_4(\cos\sigma \sin\lambda \sin\varepsilon - \cos\lambda \sin\nu \sin\sigma) \\
G_8 &= q_1 \cos\lambda \cos\sigma \sin(\nu - \varepsilon) + q_2(\cos\varepsilon \cos\sigma \sin\lambda - \cos\lambda \cos\nu \sin\sigma) \\
&\quad + q_4[\cos\lambda \cos\sigma \cos(\nu - \varepsilon) + \sin\lambda \sin\sigma] + q_3(\cos\sigma \sin\lambda \sin\varepsilon - \cos\lambda \sin\nu \sin\sigma)
\end{aligned} \tag{38}$$

Setting the determinant of $[\boldsymbol{A}]$ to zero, we obtain the algebraic equation of the singularity variety of the general 3-$\widehat{\text{RRR}}$ manipulator as

$$\begin{aligned}
\mathcal{S}: & c_1 q_1 q_2 q_3 q_4 + c_2 q_1^3 q_3 + c_3 q_2^3 q_4 + c_4 q_3^3 q_1 + c_5 q_4^3 q_2 + c_6 q_1^2 q_3^2 \\
& + c_7 q_2^2 q_4^2 + c_8 q_1^2 q_3 q_4 + c_9 q_1^2 q_2 q_3 + c_{10} q_1^2 q_2 q_4 + c_{11} q_2^2 q_3 q_4 \\
& + c_{12} q_2^2 q_1 q_3 + c_{13} q_2^2 q_1 q_4 + c_{14} q_3^2 q_2 q_4 + c_{15} q_3^2 q_1 q_2 + c_{16} q_3^2 q_1 q_4 \\
& + c_{17} q_4^2 q_1 q_2 + c_{18} q_4^2 q_2 q_3 + c_{19} q_4^2 q_1 q_3 = 0
\end{aligned} \tag{39}$$

The coefficients c_1 to c_{19} are constants defined by the positions of $\mathbf{u}_i$ and $\mathbf{v}_i$, $i = 1, 2, 3$. The singularity variety is a quartic surface in the homogeneous coordinates q_1, q_2, q_3, and q_4. Its geometric properties are a function of the parameters defining the kinematic architecture of the spherical parallel manipulator.

6.2 Singularity Varieties of Special Cases. The geometric properties of the singularity variety are characterized by the positions of the fixed and moving pivots. Besides, the above general architecture, we have studied the singularity variety of the following special architectures.

Type 1 Pivots lie on a great circle. There are three cases: (a) the fixed pivots $\mathbf{u}_1, \mathbf{u}_2$, and $\mathbf{u}_3$ lie on a great circle; (b) the moving pivots $\mathbf{v}_i$, $\mathbf{v}_2$, and $\mathbf{v}_3$ lie on a great circle; and (c) both the fixed pivots and the moving pivots lie on great circles, Fig. 8.

Table 2 The positions of pivots $\mathbf{u}_i$ and $\mathbf{v}_i$, $i = 1, 2, 3$, defined in the fixed and moving frames

	1	2	3
	$\mathbf{u}_1$	$\mathbf{u}_2$	$\mathbf{u}_3$
X	0	0	$\sin\lambda$
Y	0	$-\sin\phi$	$-\sin\nu\cos\lambda$
Z	1	$\cos\phi$	$\cos\nu\cos\lambda$
	$\mathbf{v}_1$	$\mathbf{v}_2$	$\mathbf{v}_3$
x_0	0	0	$\sin\sigma$
y_0	0	$-\sin\delta$	$-\sin\epsilon\cos\sigma$
z_0	1	$\cos\delta$	$\cos\epsilon\cos\sigma$

Type 2 Pivots are coincident. There are three cases: (a) Two of moving pivots $\mathbf{v}_i$ are coincident in the moving body, (b) two of the fixed pivots $\mathbf{u}_i$ are coincident, or (c) both fixed pivots and moving pivots are coincident, Fig. 9.

Type 3 Pivots are both coincident and on great circles. There are two cases: (a) the pivots $\mathbf{v}_i$ are on a great circle and two fixed pivots are coincident; and (b) the pivots $\mathbf{u}_i$ are on a great circle and two of the moving pivots are coincident, Fig. 10.

In what follows, we provide the singularity varieties of these cases. The positions of the pivots $\mathbf{u}_i$ and $\mathbf{v}_i$ are defined as shown in Table 3, where s and c denote the sine and cosine functions, respectively.

The pivots $\mathbf{u}_i$ *lie on a great circle*. In this case, the singularity variety of the platform is given by

$$\begin{aligned}
\mathcal{S}: & k_1 q_1^3 q_3 - k_1 q_4^3 q_2 + k_2 q_3^3 q_1 - k_2 q_2^3 q_4 + k_3 q_1^2 q_3^2 - k_3 q_2^2 q_4^2 \\
& + k_4 q_1^2 q_2 q_3 + k_5 q_2^2 q_1 q_4 + k_6 q_1^2 q_3 q_4 + k_7 q_2^2 q_3 q_4 + k_8 q_1^2 q_2 q_4 \\
& + k_9 q_2^2 q_1 q_3 + k_5 q_3^2 q_1 q_4 + k_7 q_3^2 q_1 q_2 + k_{10} q_3^2 q_2 q_4 + k_4 q_4^2 q_2 q_3 \\
& + k_6 q_4^2 q_1 q_2 + k_{11} q_4^2 q_1 q_3 = 0
\end{aligned} \tag{40}$$

where the coefficients k_i, $i = 1, \ldots 11$ are constants defined by the positions of $\mathbf{u}_i$ and $\mathbf{v}_i$, $i = 1, 2, 3$.

The pivots $\mathbf{v}_i$ *lie on a great circle*. In this case, the singularity variety of the platform is given by

$$\begin{aligned}
\mathcal{S}: & k_1 q_1^3 q_3 + k_1 q_2^3 q_4 + k_2 q_3^3 q_1 + k_2 q_4^3 q_2 + k_3 q_1^2 q_3^2 - k_3 q_2^2 q_4^2 \\
& + k_4 q_1^2 q_2 q_4 + k_5 q_2^2 q_1 q_3 + k_6 q_1^2 q_2 q_3 + k_7 q_2^2 q_1 q_4 - k_8 q_1^2 q_3 q_4 \\
& + k_9 q_2^2 q_3 q_4 + k_5 q_3^2 q_2 q_4 + k_7 q_3^2 q_1 q_4 - k_9 q_3^2 q_1 q_2 + k_4 q_4^2 q_1 q_3 \\
& + k_6 q_4^2 q_2 q_3 + k_8 q_4^2 q_1 q_2 = 0
\end{aligned} \tag{41}$$

where the coefficients k_i, $k = 1, \ldots 9$ are constants defined by the positions of $\mathbf{u}_i$ and $\mathbf{v}_i$, $i = 1, 2, 3$.

The pivots $\mathbf{u}_i$ *and* $\mathbf{v}_i$ *lie on great circles*. In this case, the singularity variety of the platform is given by

$$\mathcal{S}: k_1(q_1^2 q_3^2 - q_2^2 q_4^2) + k_2(q_1^2 q_2 q_3 + q_4^2 q_2 q_3) + k_3(q_2^2 q_1 q_4 + q_3^2 q_1 q_4) = 0 \tag{42}$$

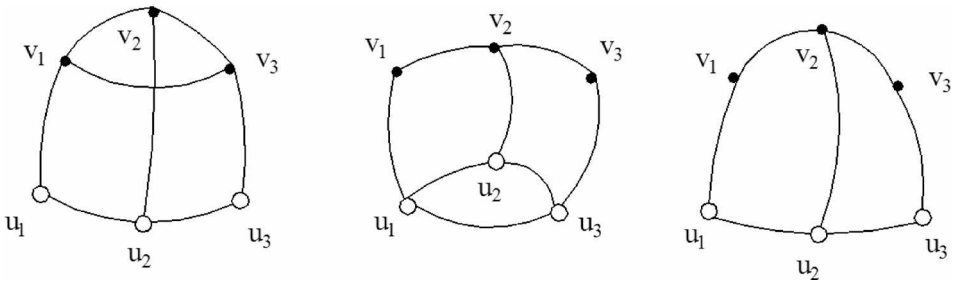

Fig. 8 Type 1: (*a*) the pivots u_i lie on a great circle, (*b*) the pivots v_i lie on a great circle, and (*c*) both sets of pivots u_i and v_i lie on great circles

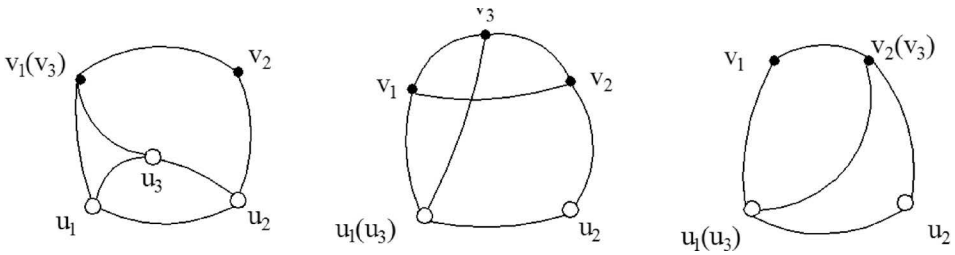

Fig. 9 Type 2: (*a*) two of the pivots v_i on the moving body are coincident, (*b*) two of the pivots u_i on the fixed body are coincident, and (*c*) there are two sets of coincident pivots on both the moving and fixed bodies

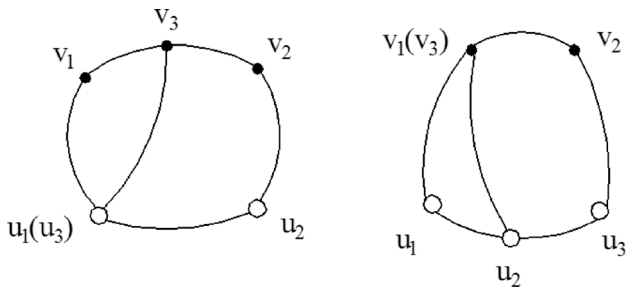

Fig. 10 Type 3: (*a*) the pivots v_i are on a great circle and two fixed pivots are coincident and (*b*) the pivots u_i are on a great circle and two of the moving pivots are coincident

where the coefficients k_i, $i = 1, 2, 3$ are constants defined by the positions of $\mathbf{u}_i$ and $\mathbf{v}_i$, $i = 1, 2, 3$.

Two of the pivots $\mathbf{v}_i$ *are coincident*. In this case, the singularity variety of the platform is given by

$$\begin{aligned}\mathcal{S}: P_1P_2 = {} & 4\sin\delta(-q_1q_3\cos\phi + q_2q_4\cos\phi + q_1q_2\sin\phi \\ & + q_3q_4\sin\phi)(q_2q_3\sin\lambda - q_1q_4\sin\lambda + q_1q_3\cos\lambda\sin\nu \\ & + q_2q_4\cos\lambda\sin\nu) = 0 \end{aligned} \tag{43}$$

Two of the pivots $\mathbf{u}_i$ *are coincident*. In this case, the singularity variety of the platform is given by

$$\begin{aligned}\mathcal{S}: P_1P_2 = {} & 4\sin\phi(q_1q_3\cos\delta + q_2q_4\cos\delta - q_1q_2\sin\delta + q_3q_4\sin\delta) \\ & \times (q_1q_3\cos\sigma\sin\varepsilon - q_2q_4\cos\sigma\sin\varepsilon + q_2q_3\sin\sigma \\ & + q_1q_4\sin\sigma) = 0 \end{aligned} \tag{44}$$

There are two sets of coincident pivots on both the moving and fixed bodies. The singularity variety of the platform is given by

$$\begin{aligned}\mathcal{S}: P_1P_2 = {} & 4\sin\phi\sin\delta(q_1q_3 - q_2q_4)(q_1q_3\cos\delta + q_2q_4\cos\delta \\ & - q_1q_2\sin\delta + q_3q_4\sin\delta) = 0 \end{aligned} \tag{45}$$

Table 3 The positions of pivots u_i and v_i, $i = 1, 2, 3$, defined in the fixed and moving frames, respectively

Type 1(a)	$\mathbf{u}_1 = (0, 0, 1)$	$\mathbf{v}_{10} = (0, 0, 1)$
	$\mathbf{u}_2 = (0, -s\phi, c\phi)$	$\mathbf{v}_{20} = (0, -s\delta, c\delta)$
	$\mathbf{u}_3 = (0, -s\nu, c\nu)$	$\mathbf{v}_{30} = (s\sigma, -s\epsilon c\sigma, c\epsilon c\sigma)$
Type 1(b)	$\mathbf{u}_1 = (0, 0, 1)$	$\mathbf{v}_{10} = (0, 0, 1)$
	$\mathbf{u}_2 = (0, -s\phi, c\phi)$	$\mathbf{v}_{20} = (0, -s\delta, c\delta)$
	$\mathbf{u}_3 = (s\lambda, -s\nu c\lambda, c\nu c\lambda)$	$\mathbf{v}_{30} = (0, -s\epsilon, c\epsilon)$
Type 1(c)	$\mathbf{u}_1 = (0, 0, 1)$	$\mathbf{v}_{10} = (0, 0, 1)$
	$\mathbf{u}_2 = (0, -s\phi, c\phi)$	$\mathbf{v}_{20} = (0, -s\delta, c\delta)$
	$\mathbf{u}_3 = (0, -s\nu, c\nu)$	$\mathbf{v}_{30} = (0, -s\epsilon, c\epsilon)$
Type 2(a)	$\mathbf{u}_1 = (0, 0, 1)$	$\mathbf{v}_{10} = (0, 0, 1)$
	$\mathbf{u}_2 = (0, -s\phi, c\phi)$	$\mathbf{v}_{20} = (0, -s\delta, c\delta)$
	$\mathbf{u}_3 = (s\lambda, -s\nu c\lambda, c\nu c\lambda)$	$\mathbf{v}_{30} = (0, 0, 1)$
Type 2(b)	$\mathbf{u}_1 = (0, 0, 1)$	$\mathbf{v}_{10} = (0, 0, 1)$
	$\mathbf{u}_2 = (0, -s\phi, c\phi)$	$\mathbf{v}_{20} = (0, -s\delta, c\delta)$
	$\mathbf{u}_3 = (0, 0, 1)$	$\mathbf{v}_{30} = (s\sigma, -s\epsilon c\sigma, c\epsilon c\sigma)$
Type 2(c)	$\mathbf{u}_1 = (0, 0, 1)$	$\mathbf{v}_{10} = (0, 0, 1)$
	$\mathbf{u}_2 = (0, -s\phi, c\phi)$	$\mathbf{v}_{20} = (0, -s\delta, c\delta)$
	$\mathbf{u}_3 = (0, 0, 1)$	$\mathbf{v}_{30} = (0, -s\delta, c\delta)$
Type 3(a)	$\mathbf{u}_1 = (0, 0, 1)$	$\mathbf{v}_{10} = (0, 0, 1)$
	$\mathbf{u}_2 = (0, -s\phi, c\phi)$	$\mathbf{v}_{20} = (0, -s\delta, c\delta)$
	$\mathbf{u}_3 = (0, 0, 1)$	$\mathbf{v}_{30} = (0, -s\epsilon, c\epsilon)$
Type 3(b)	$\mathbf{u}_1 = (0, 0, 1)$	$\mathbf{v}_{10} = (0, 0, 1)$
	$\mathbf{u}_2 = (0, -s\phi, c\phi)$	$\mathbf{v}_{20} = (0, -s\delta, c\delta)$
	$\mathbf{u}_3 = (0, -s\nu, c\nu)$	$\mathbf{v}_{30} = (0, 0, 1)$

The pivots $\mathbf{v}_i$ *are on a great circle and two fixed pivots are coincident*. In this case, the singularity variety of the platform is given by

$$\begin{aligned}\mathcal{S}: P_1P_2 = {} & 4\sin\phi\sin\varepsilon(q_1q_3 - q_2q_4)(q_1q_3\cos\delta + q_2q_4\cos\delta \\ & - q_1q_2\sin\delta + q_3q_4\sin\delta) = 0 \end{aligned} \tag{46}$$

The pivots $\mathbf{u}_i$ *are on a great circle and two of the moving pivots are coincident*. In this case, the singularity variety of the platform is given by

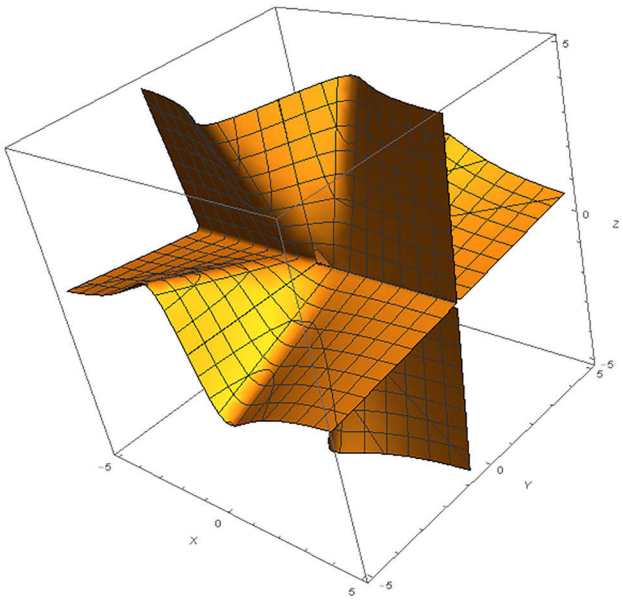

Fig. 11 The singularity variety of the 3-$\widehat{\text{RRR}}$ spherical parallel manipulator that has both sets of pivots u_i and v_i lie on great circles

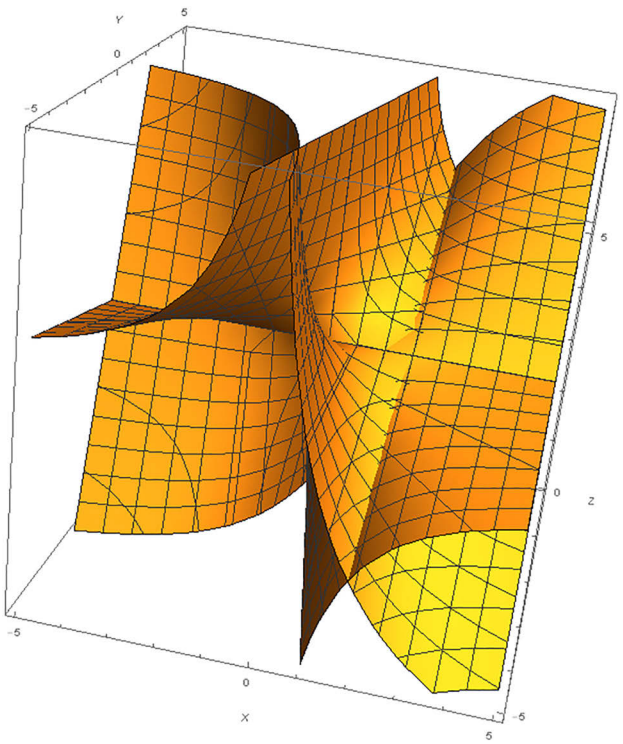

Fig. 12 The singularity variety of the 3-$\widehat{\text{RRR}}$ spherical parallel manipulator that has two coincident pivots on the base and two coincident pivots on the platform, decomposes into pairs of quadric surfaces

$$\mathcal{S}: P_1P_2 = 4\sin\nu\sin\delta(q_1q_3 + q_2q_4)(-q_1q_3\cos\phi + q_2q_4\cos\phi + q_1q_2\sin\phi + q_3q_4\sin\phi) = 0 \quad (47)$$

Notice that the quartic singularity varieties of some special cases that have coincident pivots decompose into pairs of quadric surfaces.

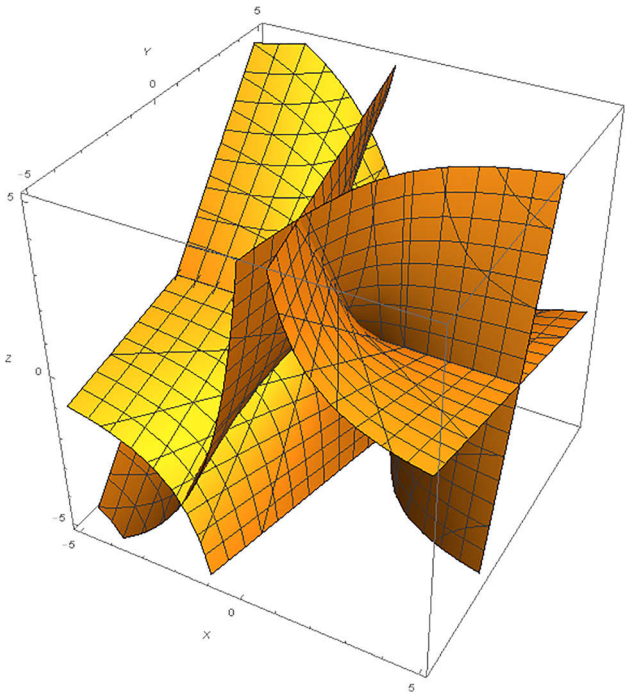

Fig. 13 The singularity variety of the 3-$\widehat{\text{RRR}}$ spherical parallel manipulator whose pivots u_i are on a great circle and two of the moving pivots are coincident, decomposes into pairs of quadric surfaces

We dehomogenize the quaternion coordinates with respect to q_4 to visualize the surfaces. This is done by making the substitution $x = q_1/q_4, y = q_2/q_4$ and $z = q_3/q_4$. For type 1(c), set $\phi = 30\,\text{deg}$, $\nu = 60\,\text{deg}$, $\delta = 30\,\text{deg}$, $\varepsilon = 60\,\text{deg}$ to obtain the quartic surface shown in Fig. 11. For type 2(c), set $\delta = 60\,\text{deg}$ to obtain the two quadric surfaces shown in Fig. 12. For type 3(b), set $\phi = 60\,\text{deg}$ to obtain the two quadric surfaces shown in Fig. 13.

7 Conclusions

In this paper, we examine two spherical parallel manipulators, 3-R‖R‖R-$\widehat{\text{RR}}$ and 3-$\widehat{\text{RRR}}$-$\widehat{\text{RR}}$, that have the property that their legs combine subchains that have specific geometric constraints. We show that these geometric constraints combine to impose hidden revolute joints in series with the RR chains that connect to the platform. Using these hidden revolute joints, the movements of the two spherical parallel manipulators are equivalent to the 3-$\widehat{\text{RRR}}$ spherical platform. A quaternion formulation provides equations for the quartic singularity varieties some of which decompose into pairs of quadric surfaces which we use to classify these spherical parallel manipulators.

This method can be used to analyze six other spherical parallel manipulators presented by Kong and Gosselin [9], specifically, the cases (i) 3-R‖R‖P-$\widehat{\text{RR}}$ (denoted 3-(RRP)^E-$\check{\text{R}}\check{\text{R}}$), (ii) 3-R‖P‖R-$\widehat{\text{RR}}$ (denoted 3-(RPR)^E-$\check{\text{R}}\check{\text{R}}$), (iii) 3-P‖R‖R-$\widehat{\text{RR}}$ (denoted 3-(PRR)^E-$\check{\text{R}}\check{\text{R}}$), (iv) 3-P‖P‖R-$\widehat{\text{RR}}$ (denoted 3-(RPP)^E-$\check{\text{R}}\check{\text{R}}$), (v) 3-P‖R‖P-$\widehat{\text{RR}}$ (denoted 3-(PRP)^E-$\check{\text{R}}\check{\text{R}}$), and (vi) 3-R‖P‖P-$\widehat{\text{RR}}$ (denoted 3-(PPR)^E-$\check{\text{R}}\check{\text{R}}$). We obtain solutions for the forward kinematic equations and present the singularity varieties of the general configuration and eight special cases. The introduction of the hidden revolute joints simplifies the kinematics and singularity analysis of these spherical parallel manipulators.

Acknowledgment

The authors gratefully acknowledge discussions with T. L. Yang and H. P. Shen of Changzhou University on type synthesis

of parallel manipulators, and the assistance of Yang Liu of the UCI Robotics and Automation Laboratory. This research was sponsored by the NSFC Grants Nos. 51405039, 51475050, and 51375062.

References

[1] Gosselin, C., Pierre, E. S., and Gagne, M., 1996, "On the Development of the Agile Eye: Mechanical Design, Control Issues and Experimentation," IEEE Rob. Autom. Mag., **3**(4), pp. 29–37.
[2] Gosselin, C., and Angeles, J., 1989, "The Optimum Kinematic Design of a Spherical Three-Degree-of-Freedom Parallel Manipulator," ASME J. Mech., Transm., Autom. Des., **111**(2), pp. 202–207.
[3] Vischer, P., and Clavel, R., 2000, "Argos: A Novel 3-DOF Parallel Wrist Mechanism," Int. J. Rob. Res., **19**(1), pp. 5–11.
[4] Di-Gregorio, R., 2001, "A New Parallel Wrist Using Only Revolute Pairs: The 3-RUU Wrist," Robotica, **19**(3), pp. 305–309.
[5] Gan, D. M., Seneviratne, L., and Dias, J., 2012, "Design and Analytical Kinematics of a Robot Wrist Based on a Parallel Mechanism," 14th International Symposium on Robotics and Applications (IEEE), Puerto Vallarta, Mexico, June 24–28, pp. 1–6.
[6] Li, T., and Payandeh, S., 2002, "Design of Spherical Parallel Mechanisms for Application to Laparoscopic Surgery," Robotica, **20**(2), pp. 133–138.
[7] Dai, J. S., Zhao, T., and Nester, C., 2004, "Sprained Ankle Physiotherapy Based Mechanism Synthesis and Stiffness Analysis of Rehabilitation Robotic Devices," Auton. Rob., **16**(2), pp. 207–218.
[8] Yang, T. L., 2004, *Topological Structure Design Theory for Robot Mechanisms*, China Machine Press, Beijing, China (in Chinese).
[9] Kong, X., and Gosselin, C. M., 2004, "Type Synthesis of 3-DOF Spherical Parallel Manipulators Based on Screw Theory," ASME J. Mech. Des., **126**(1), pp. 101–108.
[10] Innocenti, C., and Parenti-Castelli, V., 1993, "Echelon Form Solution of Direct Kinematics for the General Fully-Parallel Spherical Wrist," Mech. Mach. Theory, **28**(4), pp. 553–561.
[11] Gosselin, C. M., Sefrioui, J., and Richard, M. J., 1994, "On the Direct Kinematics of Spherical Three-Degree-of-Freedom Parallel Manipulators of General Architecture," ASME J. Mech. Des., **116**(2), pp. 594–598.
[12] Huang, Z., and Yao, Y. L., 1999, "A New Closed-Form Kinematics of the Generalized 3-DOF Spherical Parallel Manipulator," Robotica, **17**(5), pp. 475–485.
[13] Bai, S. P., Hansen, M. R., and Angeles, J., 2009, "A Robust Forward Displacement Analysis of Spherical Parallel Robots," Mech. Mach. Theory, **44**(12), pp. 2204–2216.
[14] Kong, X., and Gosselin, C. M., 2010, "A Formula That Produces a Unique Solution to the Forward Displacement Analysis of a Quadratic Spherical Parallel Manipulator: The Agile Eye," ASME J. Mech. Rob., **2**(4), p. 044501.
[15] Zhang, L., Jin, Z. L., and Li, S. Z., 2014, "Kinematics Analysis and Design of a Novel Spherical Orthogonal 3-RRR Parallel Mechanism," J. Chem. Pharm. Res., **6**(7), pp. 2470–2476.
[16] Gan, D. M., Dai, J. S., and Dias, J., 2015, "Forward Kinematics Solution Distribution and Analytic Singularity-Free Workspace of Linear-Actuated Symmetrical Spherical Parallel Manipulators," ASME J. Mech. Rob., **7**(4), p. 041007.
[17] Gosselin, C. M., and Angeles, J., 1990, "Singularity Analysis of Closed-Loop Kinematic Chains," IEEE Trans. Rob. Autom., **6**(3), pp. 281–290.
[18] Bonev, I. A., and Gosselin, C. M., 2005, "Singularity Loci of Spherical Parallel Mechanisms," IEEE Trans. Rob. Autom., pp. 2957–2962.
[19] Sefrioui, J., and Gosselin, C. M., 1995, "On the Quadratic Nature of the Singularity Curves of Planar Three-Degree-of-Freedom Parallel Manipulators," Mech. Mach. Theory, **30**(4), pp. 533–551.
[20] Collin, C. L., and McCarthy, J. M., 1998, "The Quartic Singularity Surfaces of Planar Platforms in the Clifford Algebra of the Projective Plane," Mech. Mach. Theory, **33**(7), pp. 931–944.
[21] Collin, C. L., and McCarthy, J. M., 1997, "The Singularity Loci of Two Triangular Parallel Manipulators," IEEE Transactions on Advanced Robotics (ICAR), Monterey, CA, July 7–9, pp. 473–478.
[22] Yu, J. J., Wu, K., and Zong, G. H., 2016, "A Comparative Study on Motion Characteristics of Three Two-Degree-of-Freedom Pointing Mechanisms," ASME J. Mech. Rob., **8**(2), p. 021027.
[23] Kong, X., and Gosselin, C. M., 2004, "Type Synthesis of Three-Degree-of-Freedom Spherical Parallel Manipulators," Int. J. Rob. Res., **23**(3), pp. 237–245.
[24] Herve, J. M., and Karouia, M., 2005, "Non-Overconstrained 3-DOF Spherical Parallel Manipulators of Type 3RCC, 3-CCR, 3-CRC," Robotica, **24**(1), pp. 1–10.
[25] McCarthy, J. M., and Soh, G. S., 2010, *Geometric Design of Linkages*, Springer, New York.
[26] McCarthy, J. M., 1990, *Introduction to Theoretical Kinematics*, The MIT Press, Cambridge, UK.